RESEARCH ARTICLE

How to cite: Ida Masluha, Yufis Azhar, "Improving Classification of Medical Images Using ESRGAN-Based Upscaling and MobileNetV2", Journal of Electronics, Electromedical Engineering, and Medical Informatics, vol. 7, no. 2, pp. 460-470, April 2025.

Improving Classification of Medical Images Using ESRGAN-Based Upscaling and MobileNetV2

Ida Masluha [iD], Yufis Azhar [iD]

Informatics Department, University of Muhammadiyah Malang, Malang, East Java, Indonesia

Corresponding author: Yufis Azhar (yufis@umm.ac.id).

ABSTRACT Medical image classification is an essential component in the development of computer-aided diagnosis systems. One of the main challenges in this field is the limitation of image resolution, which can negatively impact the performance of machine learning models. Low-quality images often lead to a decrease in classification accuracy, particularly in identifying critical features in sensitive cases such as skin and ocular disorders. Therefore, improving image quality is a strategic step that is highly necessary to optimize the overall performance of classification systems. Low-resolution photos are frequently problematic in the medical field when diagnosing skin and eye conditions since they can induce noise and lower the precision of classification algorithms. To overcome this, this research implements the Enhanced Super-Resolution Generative Adversarial Network (ESRGAN) method, which is used to perform upscaling, namely increasing the resolution of a low image to a high-resolution image. The research results show that ESRGAN can improve the quality of eye and skin images, as proven by accuracy consistency tests on the two datasets. For image classification, the MobileNetV2 model is used because this model is suitable for eye and skin datasets. Evaluation of the image retrieval system using a high-resolution dataset generated from ESRGAN upscaling demonstrates consistent performance, with a slight accuracy improvement of 1%, reflecting the system's robustness in maintaining reliable results across datasets. In this research, the improvement in visual image quality is also proven by the high Peak Signal-to-Noise Ratio (PSNR) value, so ESRGAN is proven effective in increasing image resolution and clarity for eye medical image datasets and skin images.

INDEX TERMS Eye disease classification, ESRGAN, MobileNetV2, PSNR, Skin disease classification.

I. INTRODUCTION

According to the World Health Organization (WHO), the definition of health includes physical balance and not just merely being free from disease [1], [2]. Visionary health is very important because the eyes play a vital role in everyday life as the main organ in the human visual system. Eye disorders can significantly reduce a person's quality of life, so attention to eye health is very important. Continuously developing medical technology has enabled early identification and treatment of various eye diseases, ultimately preventing blindness and visual impairment. Advancements in medical science and technology have played an important role in improving the community's quality of life, especially by making it easier for medical personnel to diagnose and determine the type of disease more accurately. Medical records are important documents that contain records of patient identity, examinations, treatments, and other medical

actions [3], these records play an important role as evidence in medical verification, protecting patient rights, and providing legal certainty in medical practice [4]. Innovative medical research is key to extending life expectancy and reducing mortality from diseases that were previously difficult to treat. In the image of eye and skin diseases, the development of classification methods based on medical image processing is very important to improve the accuracy of diagnosis and speed up the treatment process. One important area in medical research is medical image processing. Therefore, this research helps medical personnel to classify eye and skin diseases more quickly and effectively. The eye is the most important organ in the human visual system, and it consists of various components, such as the lens, retina, and optic nerve, which work together to process light and produce clear vision [5], [6].

Journal of Electronics, Electromedical Engineering, and Medical Informatics
Multidisciplinary: Rapid Review: Open Access Journal

Vol. 7, No. 2, April 2025, pp: 460-470; eISSN: 2656-8632

Several eye diseases can interfere with vision function. Eye disease conditions include cataracts, glaucoma, and retinal disease, the main causes of blindness [7]. Therefore, eye diseases or disorders should be detected before blindness occurs [8]. Early detection of eye disease can increase the chances of more effective treatment and prevent permanent damage to vision. However, challenges in diagnosing eye diseases often arise due to the low quality of medical images. Detecting eye disease is important enough to prevent permanent blindness, but low-resolution medical images often hinder the classification process and interfere with eye disease detection. Image upscaling technology can help improve the quality of medical images, allowing for a more accurate classification process and more effective early diagnosis.

Low-resolution images have relatively low pixel density, so a super-resolution method is needed to improve the image quality to a higher resolution so that visual information can be displayed more clearly and in detail [9]. Blurry or low-quality images can make identifying early signs of eye diseases difficult, so a technology that can significantly improve image quality is needed. This study develops an image upscaling method for detecting eye diseases to improve accurate identification and test the upscaling method. Early detection of eye diseases such as cataracts, glaucoma, and retinal disease is very important to prevent blindness, and the use of digital image processing technology, such as Convolutional Neural Network (CNN), can help in the process of classifying and identifying eye disorders with satisfactory accuracy [10].

Eye diseases are often difficult to detect early due to low image quality. Therefore, digital image processing technologies, such as Convolutional Neural Networks (CNN), can improve accuracy in classifying and identifying eye diseases. CNN can effectively classify various eye conditions, including cataracts, glaucoma, and retinal diseases, which are the primary focus of this study. However, despite the promising results, CNN models still face challenges in detecting subtle disease signs in low-resolution images, thus indicating a research gap in improving the accuracy of early-stage detection in medical image classification. Convolutional Neural Network (CNN) is a deep learning-based method that is effective in classifying diseases [11]. Using CNN for eye disease classification can improve the accuracy of diagnosis and accelerate the disease identification process [12]. This study involves the use of eye disease detection image datasets with the Convolutional Neural Network (CNN) model and MobileNetV2 architecture [13]. The development of this model can improve the identification of eye diseases.

Upscaling is the process of increasing the resolution of an image from low resolution to high resolution by estimating new pixel values based on existing pixels. In the process, the low-resolution image is mapped into a larger image [14]-[21]. In this study, the upscaling technique used is the Enhanced Super-Resolution Generative Adversarial Network (ESRGAN) method. Enhanced Super-Resolution Generative Adversarial Network (ESRGAN) is a deep learning-based model used to increase the resolution of low-quality images by producing high-quality and detailed images through

adversarial training, where the generator network creates realistic images, and the discriminator network distinguishes between the original image and the generated image [22].

This study optimized low-resolution eye images, including normal eye images, cataracts, glaucoma, and retinal diseases, by enhancing their resolution from 128x128 to 512x512 using ESRGAN. To evaluate the consistency of the upscaling method, a second test was conducted on a skin dataset. The resolution enhancement through this upscaling technique consistently improved performance, with an accuracy increase of approximately 1%. The upscaling results produced clearer images, contributing to a more effective image classification process. With improved image quality, the classification model can more accurately detect signs of various eye condition. The application of this upscaling technique is expected to make it easier for medical personnel to identify diseases, thereby helping medical professionals make more accurate decisions and improving the accuracy of deep learning models in automatic medical diagnosis [23].

II. MATERIALS AND METHODS

This study aims to implement an upscaling technique to optimize the classification of low-resolution medical images. The research focuses on utilizing ESRGAN to enhance the resolution of input images from 128x128 pixels to 512x512 pixels. With the improved image quality, the classification performance using the MobileNetV2 model is expected to achieve higher accuracy in identifying medical conditions.

A. DATASET

This study uses an image dataset for eye disease detection obtained from Kaggle as an open-source source (https://www.kaggle.com/datasets/jr2ngb/cataractdataset/data). The eye dataset consists of a total of 601 images divided into four classes, namely 'Normal' with a total of 300 images, 'Cataract' with a total of 100 images, 'Glaucoma' with a total of 101 images, and 'Retina Disease' with a total of 100 images [24]. The selection of the eye dataset with four classes tests the model's ability to detect common eye diseases to obtain accurate classification results.

While the second dataset, namely the skin dataset, consists of a total of 95 images divided into three classes, namely 'mel' with a total of 39, 'bcc' with a total of 30, 'akiec' with a total of 26 (https://www.kaggle.com/datasets/artakusuma/basedir). To improve the model's accuracy and address the imbalance in the number of images across categories, data augmentation techniques were applied. With this augmentation, the number of images in each category became more balanced: 224 images for the 'akiec' category, 228 images for the 'bcc' category, and 237 images for the 'mel' category. Data augmentation aims to generate new variations from the existing images, such as rotation, resizing, and flipping. This allows the model to be trained with a more diverse set of examples, which helps improve its accuracy in classifying images from all three categories.

FIGURE 1 shows an example of an image in this dataset [25]. Although the skin image dataset consists of seven

Journal of Electronics, Electromedical Engineering, and Medical Informatics
Multidisciplinary: Rapid Review: Open Access Journal

Vol. 7, No. 2, April 2025, pp: 460-470; eISSN: 2656-8632

classes, this test is focused on only three classes to maintain consistency and ensure that the upscaling method can be tested well on limited classes. This is done to assess the consistency and effectiveness of the upscaling method so that it can be tested and its capabilities proven not only on medical eye images but also on medical skin images.
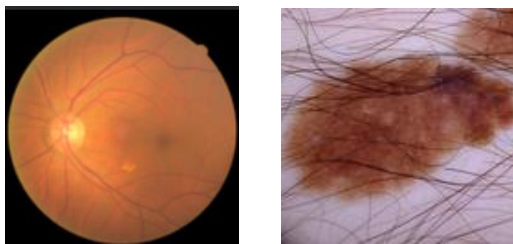
(a)   (b)

FIGURE 1. Eye images (a) and skin images (b).

B. ESRGAN UPSCALING METHOD

This study aims to enhance low-resolution images by applying the Enhanced Super-Resolution Generative Adversarial Networks (ESRGAN) method. Improving the quality of eye and skin images is very important to medical personnel, especially in determining the type of disease and its classification. FIGURE 2 illustrates the workflow of the applied method.
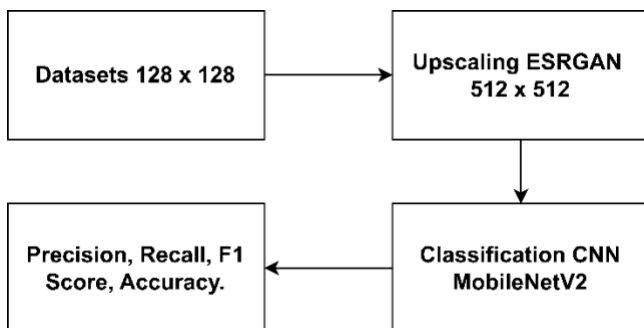

FIGURE 2. Workflow of the applied method.

The first step in this research starts from the data preprocessing stage, where the data will be processed for further preparation. Furthermore, the upscaling process is carried out from the low-resolution dataset to the high-resolution dataset to increase the image resolution of the dataset using ESRGAN [26], [27], [28] (FIGURE 3). Enhanced Super-Resolution Generative Adversarial Network (ESRGAN) is a development of the Super-Resolution Generative Adversarial Network (SRGAN), which works with two generator neural networks tasked with creating high-resolution images and a discriminator that evaluates whether the image is real or artificial [29], [30].
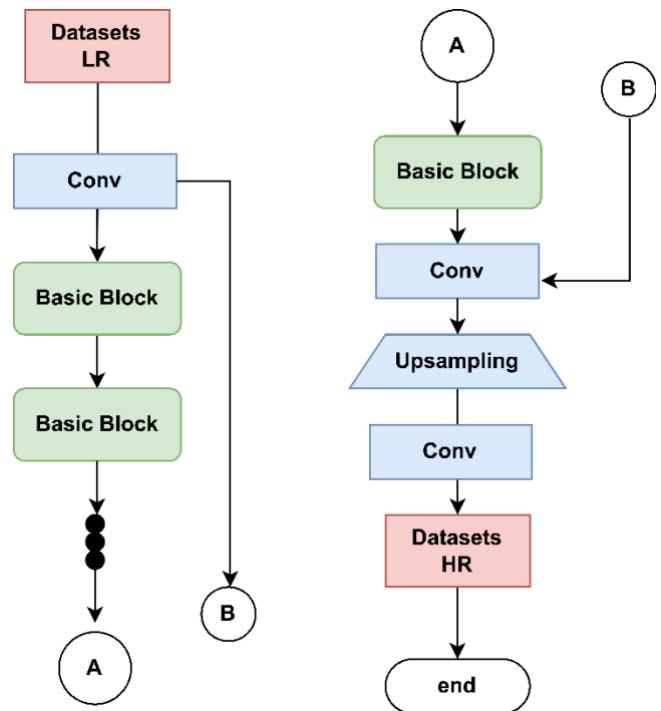

FIGURE 3. Residual in Residual Block (RRDB) ESRGAN [30].

ESRGAN is an improvement on the SRGAN method, both of which use GAN. Generative Adversarial Networks (GAN) is a framework for estimating generative models through adversarial processes [31]. The use of ESRGAN in the pre-processing process helps to improve the model's learning ability, which has a positive impact on classification accuracy [32], [33].

To train the ESRGAN model, the collected images were initially down-sampled to a resolution of 128x128 using LANCZOS. The LANCZOS interpolation function uses Eq. (1) [30]and Eq. (2) [30]as follows.

$$L(x) = sinc(x) \cdot sinc\left(\frac{x}{a}\right) \qquad (1)$$

$$sinc(x) = \frac{\sin(\pi x)}{\pi x} \qquad (2)$$

Based on Eq. (1), $(L(x))$ is a combination of two functions, where (x) serves as the input that determines the pattern, while (a) is the scaling factor that affects the width of the second function. $if\ a > 1$, the second function will widen while $if\ 0 < a < 1$, the function will narrow. Meanwhile, according to Eq. (2), the function $sinc(x)$ combines the wave pattern of $\sin(\pi x)$ with the damping effect caused by πx in its denominator. As a result, this function oscillates like a wave, but its amplitude decreases symmetrically as it moves away from the point $x = 0$.

The LANCZOS model is a down-sampling model that is suitable for upscaling techniques [34]. After that, data preprocessing was performed, and then the images were upscaled using ESRGAN to increase their resolution to 512x512.
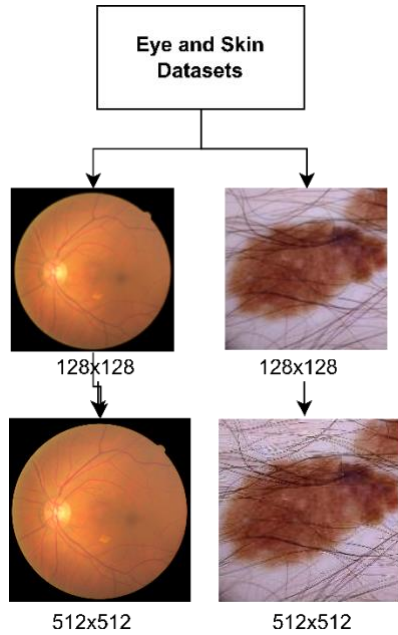
FIGURE 4. Example of the upscaling process for eyes and skin dataset.

This process produces low-resolution and high-resolution datasets generated through the ESRGAN upscaling technique (FIGURE 4). These two datasets will be compared to evaluate the effectiveness of ESRGAN in improving the performance of the image retrieval system. The comparison aims to determine whether the application of ESRGAN can improve the quality and accuracy of image retrieval. Furthermore, similar testing will also be carried out on the skin dataset. Eq. (3) [35], (4) [35], and (5) [35] are calculated to evaluate classification performance and the F1 Score.

$$F1 = 2 \cdot \frac{Precision.Recall}{Precision+Recall} \qquad (3)$$

$$Precision = \frac{True\ Positives}{True\ Positives+False\ Positives} \qquad (4)$$

$$Recall = \frac{True\ Positives}{True\ Positives+False\ Negatives} \qquad (5)$$

F1-score is a metric that combines Precision and Recall to evaluate the model's performance. Precision measures the accuracy of positive predictions, while Recall measures the model's ability to find all positive cases. F1-score provides a balance between the two, helping to minimize both false positives and false negatives. These two datasets aim to measure the consistency of accuracy improvements made using the ESRGAN upscaling technique.

C. CLASSIFICATION MODEL EVALUATION

$$X = Preprocessing(D) \qquad (6)$$

As represented by the Eq. (6) [13], where the dataset D is prepared and transformed into input data X through processes like resizing and normalization. This process ensures that the data is in the correct format for the model.

The data is divided into two parts: training and test data. The next step is model development, as in block FIGURE 5 for MobileNetv2. The model will be built based on previously prepared data. The model used in this study for image classification is the MobileNetv2 model. MobileNetV2 is a development of the MobileNetV1 architecture, which is designed to minimize resource usage while maintaining high accuracy [13].

$$F = MobileNetV2\_Base(x) \qquad (7)$$

Eq. (7) show that the input data x is passed through the MobileNetV2 convolutional layers, which extract important features F from the images. [13].
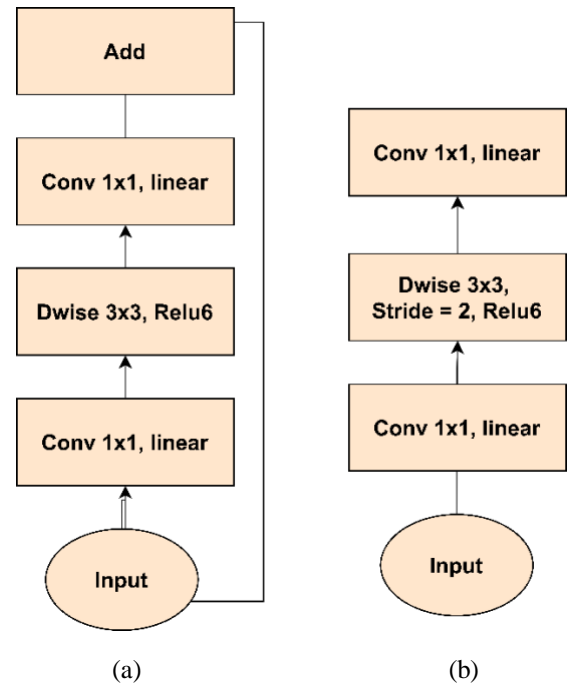

(a)   (b)

FIGURE 5. Example block for the MobileNetv2 [13] **(a) Stride = 1 Block (b) Stride = 2 Block.**

After feature extraction, Global Average Pooling (GAP) is applied to reduce the dimensionality of the feature maps while preserving important information. This pooling operation transforms the features F into a compact vector representation G as described by the Eq. (8) [13].

$$G = GlobalAvgPooling(F) \qquad (8)$$

The feature vector G is then passed through the fully connected (dense) layer to calculate the logit scores Z for each class. Where W represents the weight matrix, and b is the bias vector. b represents the bias vector, which enables the model to make necessary adjustments by incorporating a constant value into the computation, thus providing more flexibility in the learning process. These scores are computed using the Eq. (9) [13].

$$Z = W.G + b \tag{9}$$

The Softmax activation function, $(\hat{y}_k)$ represents the probability for class (k_1), calculated by comparing the score (Z_k) of that class with the scores of the other classes. Here, (Z_k) is the input value for class (k_1), typically obtained from the model's output (such as logits or values before activation). The exponential function (e^{Z_k}) is used to convert (Z_k) into a positive number and amplify differences between classes. The denominator $(\sum_{j=1}^{C} e^{Z_j})$ is the sum of the exponentials of all classes, ensuring that the total probability across all (C) classes sums to 1. In this way, Softmax converts the scores into probabilities that can be interpreted as the predicted likelihood for each class. Can be seen in Eq. (10) [31]

$$\hat{y}_k = \frac{e^{Z_k}}{\sum_{j=1}^{C} e^{Z_j}} \tag{10}$$

where L is a measure of error that shows how far the model's prediction is from the correct label. N is the number of data used for training and C is the number of available classes. $(y_{i,k})$ is the true label for class (k) of the (i)-th data point, while $(\hat{y}_{i,k})$ is the predicted probability for that class. The logarithmic function $(\hat{y}_{i,k})$ calculates the penalty given when the model makes an incorrect prediction. During training, this value is minimized, so the model makes more accurate predictions by assigning higher probabilities to the correct class. The summation is done for all the available data. The Eq. (11) [36].

$$L = -\frac{1}{N} \sum_{i=1}^{N} \sum_{k=1}^{C} y_{i,k} \log(\hat{y}_{i,k}) \tag{11}$$

Classification using Convolutional Neural Network (CNN) with the MobileNetV2 model in this study aims to help medical personnel determine the types of diseases more easily and utilize transfer learning to increase time efficiency [37]. With transfer learning, the model can be trained faster, using knowledge from the previous model, thereby speeding up the diagnosis process and helping to detect eye diseases more accurately.

III. RESULT

Before the training process begins, the images in the dataset are down-sampled to a resolution of 128x128 pixels using the Lanczos method, a 'sinc' filter-based interpolation technique. This method is very effective for down-sampling because it can better maintain the sharpness and smoothness of the image. The Lanczos filter is a 'sinc' kernel-based interpolation method used for resampling digital signals, known for its ability to produce smooth and sharp interpolations, as well as reduce artifacts [38]. ESRGAN uses a Residual-in-Residual Dense Block (RRDB) as the basic unit without batch normalization, which increases the capacity and ease of training deeper networks [39], [40]. ESRGAN model training is performed with various hyperparameter adjustments to ensure the model runs optimally and efficiently. After the ESRGAN model is trained, the resulting high-resolution images show significant quality improvement compared to low-resolution input images. The ESRGAN model can enhance important details in eye and skin disease images,

preserving intricate patterns and textures for accurate image classification and retrieval.

$$PSNR = 10 log_{10} \left(\frac{(L-1)}{MSE} \right)^2 = 20 log_{10} \left(\frac{L-1}{RMSE} \right) \tag{12}$$

According to Eq. (12) [41], Peak Signal-to-Noise Ratio (PSNR) is a metric used to measure the quality of a reconstructed image by comparing it to the original image. L is the maximum pixel intensity value, MSE or Mean Squared Error is the average of the squared pixel differences between the original and reconstructed images, and RMSE or Root Mean Squared Error is the root of MSE, which is used to adjust the units to the original image. PSNR is very important in image processing, especially when assessing the effectiveness of image upscaling techniques.

The formula works as follows: The first part explains that PSNR is calculated by multiplying 10 by the base-10 logarithm of the ratio between the square of the maximum pixel intensity value and the MSE. A higher PSNR value indicates better image reconstruction or compression quality. The second part of the formula is an alternative form that uses RMSE, the square root of MSE, in the calculation. The factor of 20 in this formula comes from using the logarithm twice for the square of the MSE error.

The results of evaluating the quality of the resulting image are measured using the PSNR metric, which is used to assess image quality based on the level of distortion. The average PSNR score achieved by the model on the eye dataset is 41.92 dB, while on the skin dataset, it is 37.64 dB. The MSE value on the eye image dataset is 63989.00, and on the skin dataset, it is 64212.17. A high PSNR score indicates better image quality and less distortion [42], [43], [44]. This indicates a high level of similarity between the generated image and the original high-resolution image.

FIGURES 6 and FIGURE 7 show that the resulting high-resolution images (on the right) show much superior clarity and detail compared to the low-resolution images (on the left). The ESRGAN model successfully recovers fine details and textures from the eye and skin disease images. With this increased resolution, small elements previously hidden in the low-resolution images are now more visible, making classification easier by the deep learning model. This upscaling result visually represents disease detection and medical diagnosis as a whole.
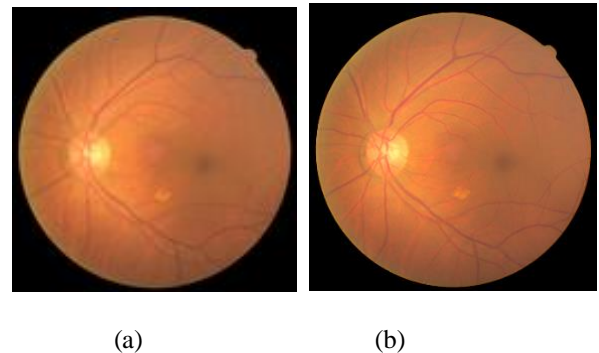

(a)   (b)

FIGURE 6. Eye images before (a) and after (b) upscaling.
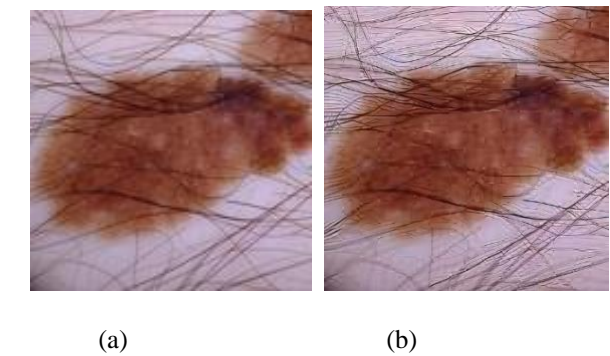
(a)   (b)

FIGURE 7. Skin images before (a) and after (b) upscaling.

Testing was conducted using the ESRGAN method's upscaling technique, and classification was done using the CNN MobileNetV2 model. Tables I and II show the testing results using the previously mentioned models. TABLE 1 presents the classification test results of the eye image dataset before and after ESRGAN-based upscaling. Before upscaling, the overall model accuracy was 0.63, while after upscaling, it only slightly increased to 0.64. In the 'normal' class, the model initially had a precision of 0.59, recall of 0.93, and F1-score of 0.73. After upscaling, precision increased to 0.64, while recall decreased to 0.85, resulting in the F1-score remaining at 0.73.

For the 'cataract' class, the model achieved a precision of 0.74, recall of 0.81, and an F1-score of 0.77 before upscaling. After upscaling, precision slightly changed to 0.76, with recall and F1-score both remaining at 0.76. In the 'glaucoma' class, before upscaling, the model had a precision of 0.80, recall of 0.19, and an F1-score of 0.31. After upscaling, precision significantly improved to 1.00, but recall decreased to 0.14, resulting in the F1-score dropping to 0.25.

In the 'retina_disease' class, the model was unable to detect the condition before upscaling (precision, recall, and F1-score all were 0.00). After upscaling, there was a performance improvement, with precision reaching 0.42, recall 0.38, and F1-score 0.40. Overall, these results indicate that ESRGAN-based upscaling has a varying impact on each disease class. While it can enhance image quality, its effect on classification performance heavily depends on the specific disease being classified.

TABLE 1
Test results for eye image dataset

Class	Before Upscaling			After Upscaling		
	p	R	F1-S	P	R	F1-S
1_normal	0.59	0.93	0.73	0.64	0.85	0.73
2_cataract	0.74	0.81	0.77	0.76	0.76	0.76
3_glaucoma	0.80	0.19	0.31	1.00	0.14	0.25
4_retina_disease	0.00	0.00	0.00	0.42	0.38	0.40
accuracy		0.63			0.64	

TABLE 2
Test Results for Skin Image Dataset

Class	Before Upscaling			After Upscaling		
	p	R	F1-S	P	R	F1-S
akiec	0.95	0.89	0.89	0.90	0.98	0.94
bcc	0.90	0.96	0.96	0.94	0.94	0.94
mel	0.94	0.94	0.94	0.98	0.90	0.94
accuracy		0.93			0.94	

TABLE 2 shows the classification test results for the skin image dataset, illustrating the impact of ESRGAN-based upscaling on the model's performance. Before upscaling, the overall model accuracy was 0.93, with varying results across different classes. In the 'akiec' class, precision was 0.95, recall 0.89, and F1-score 0.89. After upscaling, precision slightly decreased to 0.90, recall increased to 0.98, and the F1-score rose to 0.94, indicating improved performance in detecting this class.

For the 'bcc' class, the model initially had precision of 0.90, recall 0.96, and F1-score 0.96. After upscaling, precision slightly increased to 0.94, while recall and F1-score remained unchanged at 0.94, indicating that upscaling had no significant impact on this class. In the 'mel' class, before upscaling, precision was 0.94, recall 0.94, and F1-score 0.94. After upscaling, precision increased to 0.98, while recall decreased to 0.90, and F1-score remained at 0.94, showing improved precision despite a slight decrease in recall.

The overall accuracy increased from 0.93 to 0.94 after ESRGAN-based upscaling, reflecting a slight improvement in the model's performance. These results demonstrate that upscaling through ESRGAN enhances the model's ability to identify features, especially for the 'akiec' class. While the impact on some classes, such as 'bcc', is relatively small, upscaling provides significant improvement in other classes, such as 'mel', leading to better feature detection and classifications.

Confusion Matrix

Actual	1_normal	93.44% (±6.21)	6.56% (±6.21)	0.00% (±0.00)	0.00% (±0.00)
	2_cataract	19.05% (±16.80)	80.95% (±16.80)	0.00% (±0.00)	0.00% (±0.00)
	3_glaucoma	80.95% (±16.80)	0.00% (±0.00)	19.05% (±16.80)	0.00% (±0.00)
	4_retina_dise ase	85.71% (±14.97)	9.52% (±12.56)	4.76% (±9.11)	0.00% (±0.00)

Predicted

FIGURE 8. Confusion matrix for eye dataset before upscaling

Journal of Electronics, Electromedical Engineering, and Medical Informatics
Multidisciplinary: Rapid Review: Open Access Journal

Vol. 7, No. 2, April 2025, pp: 460-470; eISSN: 2656-8632

Overall, ESRGAN-based upscaling consistently improves the model's performance, with an accuracy increase of approximately 0.01 (1%) across both datasets. This proves that this upscaling technique is reliable in enhancing image quality and classification accuracy for skin disease images. FIGURE 8 shows the model's prediction results for the eye disease dataset before upscaling. This dataset consists of four categories: '1_normal', '2_cataract', '3_glaucoma', and '4_retina_disease'. The model performed well in classifying '1_normal' images, correctly identifying 93.44% of the images as normal. However, some images from the '1_normal' class were misclassified as '2_cataract', accounting for 6.56%. This indicates that the model struggles to differentiate between healthy eyes and those showing early signs of cataracts. The margin of ±6.21% reflects the level of uncertainty or variation in the model's predictions, meaning the error rate can vary around this value.

For the '2_cataract' class, the model correctly classified 80.95% of the images as cataracts, but 19.05% of the images from this class were misclassified as '1_normal'. This suggests that the model has difficulty recognizing cataract features, which may resemble normal eye images. The margin of ±16.80% indicates that misclassifications are more frequent in this class, likely due to the visual similarities between cataracts and healthy eyes.

The model's performance for the '3_glaucoma' class was poor, with only 19.05% of images correctly classified as '3_glaucoma'. The remaining 80.95% were misclassified, including 6.56% predicted as '1_normal' and 19.05% as '2_cataract'. No images were predicted as '4_retina_disease'. The margin of ±16.80% shows that the model faces challenges in recognizing glaucoma features, such as optic nerve damage, which are difficult to detect in low-resolution images.

For the '4_retina_disease' class, the model correctly identified 85.71% of the images. However, 9.52% of the images were misclassified as '1_normal', and 4.76% as '2_cataract'. No images were predicted as '3_glaucoma'. The margin of ±14.97% in this class indicates that, although the model is better at identifying retinal disease, there are still misclassifications that need to be addressed.

Overall, the model performs better in identifying '1_normal' images but struggles with detecting diseases such as cataracts, glaucoma, and retinal disease. Misclassifications are more frequent between disease classes, highlighting the need for improved recognition of specific disease features, particularly for glaucoma and cataracts. The model's performance could be improved by using higher-resolution images and better feature extraction techniques to handle the subtle visual differences between disease classes. Reducing the margin or uncertainty in these classifications could help increase the model's accuracy.

FIGURE 9 shows the results of the confusion matrix after the image upscaling process for eye condition classification. This matrix provides an overview of how well the model predicted eye conditions by showing the number of correct and incorrect predictions for each category. The four eye condition categories tested are '1_normal', '2_cataract', '3_glaucoma', and '4_retina_disease'.
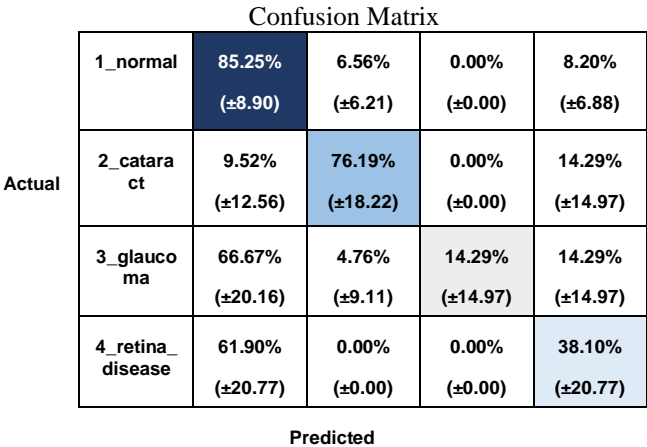
Confusion Matrix

	1_normal	85.25% (±8.90)	6.56% (±6.21)	0.00% (±0.00)	8.20% (±6.88)
	2_cataract	9.52% (±12.56)	76.19% (±18.22)	0.00% (±0.00)	14.29% (±14.97)
Actual	**3_glaucoma**	66.67% (±20.16)	4.76% (±9.11)	14.29% (±14.97)	14.29% (±14.97)
	4_retina_disease	61.90% (±20.77)	0.00% (±0.00)	0.00% (±0.00)	38.10% (±20.77)

Predicted

FIGURE 9. Confusion matrix for eye dataset after upscaling

In the '1_normal' class, the model correctly classified 85.25% of images as '1_normal'. However, there were some misclassifications, with 6.56% of images being incorrectly predicted as '2_cataract', 8.20% as '4_retina_disease', and no images predicted as '3_glaucoma'. This suggests that while the model was accurate in recognizing healthy eyes, it still struggled to distinguish between healthy eyes and those showing early signs of other conditions, such as cataracts and retina diseases. The margin of ±8.90% indicates a reasonable variation in the predictions.

For the '2_cataract' class, the model correctly classified 76.19% of images as '2_cataract'. However, 9.52% were misclassified as '1_normal' and 14.29% as '4_retina_disease'. This indicates that the model had difficulty recognizing the characteristic patterns of cataracts, which might resemble healthy eye images or signs of retina disease. The margin of ±18.22% reflects a higher level of uncertainty in predictions for this class.

For the '3_glaucoma' class, the model correctly classified 66.67% of images as '3_glaucoma'. However, 4.76% were misclassified as '2_cataract', 14.29% as '1_normal', and 14.29% as '4_retina_disease'. These misclassifications suggest that the model struggled to recognize the distinctive features of glaucoma, such as optic nerve damage, which may be too subtle to detect with the image data used. The margin of ±20.16% indicates significant variation in the predictions for this class.

In the '4_retina_disease' class, the model correctly classified 61.90% of images as '4_retina_disease'. However, there were misclassifications, with 38.10% of images predicted as '1_normal'. No images were predicted as '2_cataract' or '3_glaucoma', indicating that the model had difficulty recognizing the specific features of retina diseases, such as abnormal blood vessel patterns or tissue damage. The margin of ±20.77% suggests considerable uncertainty in the predictions for this class.

Overall, while the model performed better in identifying healthy eyes as '1_normal', it struggled with classifying other eye conditions such as cataracts, glaucoma, and retina diseases. This may be due to difficulties in distinguishing between visually similar features across conditions or insufficient data to adequately represent each class. The

margin of variation indicates uncertainty in the model's predictions, which could be reduced with better data or more advanced feature extraction techniques.

FIGURE 10. Confusion matrix for skin dataset before upscaling

FIGURE 10 presents the model's performance in classifying different types of skin diseases prior to the upscaling of the data. The model was tested on three different classes: 'akiec', 'bcc', and 'mel'. In the 'akiec' class, the model was able to correctly classify 41 images as 'akiec'. However, there were some misclassifications, with 3 images being incorrectly identified as 'bcc' and 2 images as 'mel'. These errors suggest that the model faces difficulties in distinguishing 'akiec' from the other conditions, particularly 'bcc' and 'mel', especially when the images have similar visual features.

In the 'bcc' class, the model correctly identified 45 images as 'bcc', indicating that it was generally successful at identifying this condition. However, it still made some misclassifications, with 1 image being wrongly identified as 'akiec' and another misclassified as 'mel'. These misclassifications indicate that, while the model performs well in identifying 'bcc', it still has difficulty differentiating it from 'mel', as the two conditions may appear visually similar in the images.

In the 'mel' class, the model performed relatively well, correctly classifying 46 images as 'mel'. Nevertheless, the model also misclassified 1 image as 'akiec' and 2 images as 'bcc'. This demonstrates that although the model performs better in identifying 'mel', it still encounters challenges, particularly when distinguishing it from 'akiec' and 'bcc'.

Overall, the model exhibits a relatively high error rate, particularly in classifying the 'akiec' and 'bcc' classes. This suggests that the model needs further refinement and improvement. Possible solutions to enhance its performance include incorporating more training data or applying more advanced techniques to improve the model's accuracy and its ability to differentiate between similar skin conditions effectively.

FIGURE 11 shows the confusion matrix results for skin disease classification after the data upscaling process. This matrix illustrates the model's accuracy and misclassification errors for three skin disease categories 'akiec', 'bcc', and 'mel'. The Margin of Error (MoE) values represent the variation in predictions for each class.

In the 'akiec' class, the model correctly classified 97.83% of the images as 'akiec'. However, 2.17% of the images were misclassified as 'bcc'. The margin of error for this class is ±4.21%, indicating a small variation in the model's ability to differentiate between 'akiec' and 'bcc'. This suggests that while the model performs well in recognizing 'akiec', it still struggles to distinguish it from 'bcc'.

FIGURE 11. Confusion matrix for skin dataset after upscaling

In the 'bcc' class, the model correctly classified 93.62% of the images as 'bcc'. However, 4.26% were misclassified as 'akiec', and 2.13% as 'mel'. The margin of error for this class is ±6.99%, indicating a higher level of uncertainty in classifications for this category. The model's difficulty distinguishing 'bcc' from 'akiec' and 'mel' highlights the need for better differentiation techniques.

In the 'mel' class, the model correctly classified 89.80% of the images as 'mel'. However, 6.12% were misclassified as 'akiec', and 4.08% as 'bcc'. The margin of error for this class is ±8.48%, which is higher compared to the other two classes. This suggests significant challenges in distinguishing 'mel' from 'akiec' and 'bcc', likely due to visual similarities between the three classes or insufficient training data.

Overall, the upscaling process has helped improve the model's performance, especially for the 'bcc' and 'mel' classes, as reflected by the relatively high classification accuracy. However, the model still struggles to distinguish the 'akiec' class from the other two. The existing margin of error reflects uncertainty in the model's predictions, particularly in the 'bcc' and 'mel' classes. To improve accuracy, particularly for the 'akiec' class, better learning techniques or a more diverse training dataset may be required to reduce misclassification rates and margin of error.

IV. DISCUSSION

The results of this study provide very important insights into the impact of applying ESRGAN-based upscaling techniques to medical image datasets, especially for the classification of eye and skin diseases. This upscaling technique increases the image resolution from 128x128 pixels to 512x512 pixels, ultimately improving the model's classification performance. This improvement plays an important role in image quality to help deep learning models recognize visual patterns that support more accurate disease detection.

On the eye disease dataset, the overall accuracy increased slightly from 63% to 64% after upscaling, indicating a modest improvement in the model's ability to recognize patterns in high-resolution images. Specifically, in the '1_normal' class, although precision (P) increased from 0.59 to 0.64 and recall (R) decreased from 0.93 to 0.85, the F1 score remained unchanged at 0.73. This suggests that while high-resolution images allow the model to detect finer details, it did not significantly impact the identification of this class. The '4_retina_disease' class showed noticeable improvement, with the F1 score rising from 0.00 to 0.40 after upscaling, although precision and recall remained relatively low at 0.42 and 0.38, indicating that higher resolution had a slight positive effect on the model's performance in identifying this class.

However, the '3_glaucoma' class showed unsatisfactory results after upscaling, despite precision increasing from 0.80 to 1.00, while recall decreased from 0.19 to 0.14. This may be due to overfitting or changes in the characteristics of the class after upscaling, suggesting that simply increasing resolution is not enough to improve performance in this class without further adjustments in training or data augmentation strategies.

On the skin disease dataset, the overall accuracy increased slightly from 93% to 94%. The largest improvement was seen in the 'mel' class, where the F1 score remained stable at 0.94, although precision increased from 0.94 to 0.98 and recall decreased slightly from 0.94 to 0.90. The 'bcc' class showed no significant change, with the F1 score remaining at 0.96, indicating that upscaling had little effect on the model's performance for this class. On the other hand, the 'akiec' class showed a significant improvement, with the F1 score rising from 0.89 to 0.94, indicating a large enhancement after upscaling.

These observations emphasize how dataset characteristics can affect model performance. Classes with more data, such as '1_normal' and 'bcc', showed larger improvements after upscaling compared to classes with smaller datasets, like '3_glaucoma' and '4_retina_disease'. This highlights the importance of addressing data imbalance through techniques like data augmentation to ensure more consistent model performance across all classes.

This research is consistent with previous research regarding the success of ESRGAN in improving image quality, especially in medical fields such as histopathology [45]. The research shows that the model becomes more effective at recognizing important details after applying super-resolution techniques. However, the results of this study also reveal that the impact of upscaling techniques can increase accuracy and consistency depending on the type of dataset used. For example, one study explains that on medical datasets with more complex images, using a more efficient model architecture such as EfficientNet provides better results [46]. This is different from this research, which only used MobileNetV2. Therefore, using more sophisticated models such as EfficientNet can improve classification performance on medical datasets. Thus, it is possible that classification performance can be further improved by switching model architectures or trying different combinations of upscaling techniques.

Another limitation is that one super-resolution technique, ESRGAN, and one classification model, MobileNetV2, are used. Although ESRGAN effectively improves image quality, exploring alternative methods such as SRGAN or bicubic interpolation may provide additional insight into the best approach for upscaling medical images. Likewise, using more sophisticated classifiers such as EfficientNet can improve performance on high-resolution datasets. In addition. Although PSNR provides a quantitative measure of distortion, this metric does not always correlate with classification performance.

The implications of this study are highly significant, especially in the field of medical imaging and disease detection. Enhancing the resolution of medical images can support better diagnosis by allowing deep learning models to identify subtle patterns that may be missed in lower-resolution images. However, it is essential to address the limitations associated with certain diseases, such as glaucoma, where resolution enhancement alone may not be enough. Future research could focus on exploring alternative upscaling methods and incorporating more diverse data augmentation strategies to further improve model robustness. Additionally, incorporating more advanced neural network architectures that specialize in medical image classification could enhance performance across all disease classes. This research encourages further exploration into combining various image enhancement techniques with cutting-edge model architectures to improve the accuracy and reliability of AI-driven medical image analysis.

V. CONCLUSION

The conclusion of this study shows that the use of the Enhanced Super-Resolution Generative Adversarial Network (ESRGAN) method successfully increases the resolution of low-resolution images into high-resolution images with sharper details and clearer textures in medical image datasets, especially for the detection of eye and skin diseases. By using ESRGAN, the image quality that was initially 128x128 pixels was successfully increased to 512x512 pixels, which had a positive impact on the classification accuracy using the MobileNetV2 model. The test results show a consistent increase in classification accuracy of 1% after applying the upscaling technique, with the final accuracy on the eye dataset reaching 64% and the skin dataset reaching 94%. A high PSNR metric indicates better image quality and minimal distortion, indicating that ESRGAN is effective in improving image detail and clarity. The PSNR and MSE results obtained for the eye dataset were respectively 41.92 dB and the MSE value was 63989.00. In the skin dataset, PSNR is 37.64 dB and MSE is 64212.17. These results show that ESRGAN effectively improves image detail and clarity, and improves the visual quality of medical images. The upscaling technique used in this study can improve the accuracy and consistency of classification in eye and skin datasets. The improvement in the quality of the resulting image also provides direct benefits for medical personnel because it helps medical personnel in a

Journal of Electronics, Electromedical Engineering, and Medical Informatics
Multidisciplinary: Rapid Review: Open Access Journal

Vol. 7, No. 2, April 2025, pp: 460-470; eISSN: 2656-8632

more accurate diagnosis process, so it is expected to increase efficiency and effectiveness in medical decision-making. Therefore, this method is expected to contribute to accelerating disease detection accurately and precisely.

REFERENCES

[1] J. Hou *et al.*, "Harnessing electronic health records for real-world evidence," Nov. 2022, doi: 10.48550/arXiv.2211.16609.

[2] S. M. Shah and R. A. Khan, "Secondary Use of Electronic Health Record: Opportunities and Challenges," *IEEE Access*, vol. 8, pp. 136947–136965, Jan. 2020, doi: 10.1109/ACCESS.2020.3011099.

[3] F. Gong, M. Wang, H. Wang, S. Wang, and M. Liu, "SMR: Medical Knowledge Graph Embedding for Safe Medicine Recommendation," *Big Data Research*, vol. 23, Oct. 2017, doi: 10.1016/j.bdr.2020.100174.

[4] B. Hettige, W. Wang, Y. F. Li, S. Le, and W. Buntine, "$\mathtt{MedGraph:}$ Structural and Temporal Representation Learning of Electronic Medical Records," *Frontiers in Artificial Intelligence and Applications*, vol. 325, pp. 1810–1817, Dec. 2019, doi: 10.3233/FAIA200296.

[5] D. Diethei, A. Colley, L. Dannenberg, M. F. J. Malik, and J. Schöning, "The Usability and Trustworthiness of Medical Eye Images," May 2021, doi: 10.48550/arXiv.2105.12651.

[6] R. Chen *et al.*, "EyeDiff: text-to-image diffusion model improves rare eye disease diagnosis," Nov. 2024, doi: 10.48550/arXiv.2411.10004.

[7] Y. Huang, L. Lin, P. Cheng, J. Lyu, R. Tam, and X. Tang, "Identifying the key components in ResNet-50 for diabetic retinopathy grading from fundus images: a systematic investigation," *Diagnostics*, vol. 13, no. 10, Oct. 2021, doi: 10.3390/diagnostics13101664.

[8] A. I Salsabila, A. P Gandasubrata, and M. Rifada, "Clinical Characteristics and Managements of Primary Open-Angle Glaucoma Patients at National Eye Center, Cicendo Eye Hospital, Bandung, Indonesia," *Journal of Medicine and Health*, vol. 5, no. 1, pp. 43–55, Feb. 2023, doi: 10.28932/JMH.V5I1.4265.

[9] X. Bing, W. Zhang, L. Zheng, and Y. Zhang, "Medical Image Super Resolution Using Improved Generative Adversarial Networks," *IEEE Access*, vol. 7, pp. 145030–145038, 2019, doi: 10.1109/ACCESS.2019.2944862.

[10] M. Elkholy and M. A. Marzouk, "Deep learning-based classification of eye diseases using Convolutional Neural Network for OCT images," *Front Comput Sci*, vol. 5, 2023, doi: 10.3389/FCOMP.2023.1252295.

[11] T. Babaqi, M. Jaradat, A. E. Yildirim, S. H. Al-Nimer, and D. Won, "Eye Disease Classification Using Deep Learning Techniques," Jul. 2023, doi: 10.48550/arXiv.2307.10501.

[12] S. Subramanian and L. H. Gilpin, "Convolutional Neural Network Model for Diabetic Retinopathy Feature Extraction and Classification," Oct. 2023, doi: 10.48550/arXiv.2310.10806.

[13] M. Sandler, A. Howard, M. Zhu, A. Zhmoginov, and L. C. Chen, "MobileNetV2: Inverted Residuals and Linear Bottlenecks," *Proceedings of the IEEE Computer Society Conference on Computer Vision and Pattern Recognition*, pp. 4510–4520, Jan. 2018, doi: 10.1109/CVPR.2018.00474.

[14] W. Sun and Z. Chen, "Learned Image Downscaling for Upscaling using Content Adaptive Resampler," *IEEE Transactions on Image Processing*, vol. 29, pp. 4027–4040, Jul. 2019, doi: 10.1109/TIP.2020.2970248.

[15] L. Wang, Z. Lin, X. Deng, and W. An, "Multi-frame image super-resolution with fast upscaling technique," Jun. 2017, doi: 10.48550/arXiv.1706.06266.

[16] N. Gat, S. Benaim, and L. Wolf, "Identity and Attribute Preserving Thumbnail Upscaling," *Proceedings - International Conference on Image Processing, ICIP*, vol. 2021-September, pp. 2708–2712, May 2021, doi: 10.1109/ICIP42928.2021.9506290.

[17] S. You *et al.*, "Enhancing digital core image resolution using optimal upscaling algorithm: with application to paired SEM images," Sep. 2024, doi: 10.48550/arXiv.2409.03265.

[18] J. Menick and N. Kalchbrenner, "Generating High Fidelity Images with Subscale Pixel Networks and Multidimensional Upscaling," *7th International Conference on Learning Representations, ICLR 2019*, Dec. 2018, doi: 10.48550/arXiv.1812.01608.

[19] R. Rombach, A. Blattmann, D. Lorenz, P. Esser, and B. Ommer, "High-Resolution Image Synthesis with Latent Diffusion Models," *Proceedings of the IEEE Computer Society Conference on Computer Vision and Pattern Recognition*, vol. 2022-June, pp. 10674–10685, Dec. 2021, doi: 10.1109/CVPR52688.2022.01042.

[20] R.-Y. Ju, C.-C. Chen, J.-S. Chiang, Y.-S. Lin, W.-H. Chen, and C.-T. Chien, "Resolution Enhancement Processing on Low Quality Images Using Swin Transformer Based on Interval Dense Connection Strategy," Mar. 2023, doi: 10.48550/arXiv.2303.09190.

[21] Y. Li, C. Chang, Z. Wang, and G. Zhao, "Upscaling remote sensing inversion and dynamic monitoring of soil salinization in the Yellow River Delta, China," *Ecol Indic*, vol. 148, p. 110087, Apr. 2023, doi: 10.1016/J.ECOLIND.2023.110087.

[22] X. Wang, L. Xie, C. Dong, and Y. Shan, "Real-ESRGAN: Training Real-World Blind Super-Resolution with Pure Synthetic Data," *Proceedings of the IEEE International Conference on Computer Vision*, vol. 2021-October, pp. 1905–1914, 2021, doi: 10.1109/ICCVW54120.2021.00217.

[23] G. Alwakid, W. Gouda, and M. Humayun, "Enhancement of Diabetic Retinopathy Prognostication Using Deep Learning, CLAHE, and ESRGAN," *Diagnostics*, vol. 13, no. 14, Jul. 2023, doi: 10.3390/DIAGNOSTICS13142375.

[24] YiWei Chen, "cataract dataset," 2019. Accessed: Nov. 23, 2024. [Online]. Available: https://www.kaggle.com/datasets/jr2ngb/cataractdataset/data

[25] Arta Kusuma, "HAM10000 Preprocessed Data," 2018. Accessed: Nov. 24, 2024. [Online]. Available: https://www.kaggle.com/datasets/artakusuma/basedir

[26] C. D. Watson, C. Wang, T. Lynar, and K. Weldemariam, "Investigating two super-resolution methods for downscaling precipitation: ESRGAN and CAR," Dec. 2020, doi: 10.48550/arXiv.2012.01233.

[27] J. Liu and N. P. Chandrasiri, "CA-ESRGAN: Super-Resolution Image Synthesis Using Channel Attention-Based ESRGAN," *IEEE Access*, vol. 12, pp. 25740–25748, 2024, doi: 10.1109/ACCESS.2024.3363172.

[28] A. Aghelan and M. Rouhani, "Fine-tuned Generative Adversarial Network-based Model for Medical Image Super-Resolution," Nov. 2022, doi: 10.48550/arXiv.2211.00577.

[29] M. I. A. Rohim *et al.*, "Peningkatan Performa Pengenalan Wajah pada Gambar Low-Resolution Menggunakan Metode Super-Resolution," *Jurnal Teknologi Informasi dan Ilmu Komputer*, vol. 11, no. 1, pp. 199–208, Feb. 2024, doi: 10.25126/JTIIK.20241117947.

[30] X. Wang *et al.*, "ESRGAN: Enhanced Super-Resolution Generative Adversarial Networks," *Lecture Notes in Computer Science (including subseries Lecture Notes in Artificial Intelligence and Lecture Notes in Bioinformatics)*, vol. 11133 LNCS, pp. 63–79, Sep. 2018, doi: 10.1007/978-3-030-11021-5_5.

[31] I. J. Goodfellow *et al.*, "Generative Adversarial Networks," *Sci Robot*, vol. 3, no. January, pp. 2672–2680, Jun. 2014, doi: 10.48550/arXiv.1406.2661.

[32] G. Alwakid, W. Gouda, and M. Humayun, "Deep Learning-Based Prediction of Diabetic Retinopathy Using CLAHE and ESRGAN for Enhancement," *Healthcare*, vol. 11, no. 6, p. 863, Mar. 2023, doi: 10.3390/HEALTHCARE11060863.

[33] J. Song, H. Yi, W. Xu, X. Li, B. Li, and Y. Liu, "ESRGAN-DP: Enhanced super-resolution generative adversarial network with adaptive dual perceptual loss," *Heliyon*, vol. 9, no. 4, p. e15134, Apr. 2023, doi: 10.1016/J.HELIYON.2023.E15134.

[34] R. C. Bituin and R. Antonio, "Ensemble Model of Lanczos and Bicubic Interpolation with Neural Network and Resampling for Image Enhancement," *ACM International Conference Proceeding Series*, pp. 110–115, Jan. 2024, doi: 10.1145/3647722.3647739/ASSETS/HTML/IMAGES/IMAGE2.PNG.

[35] D. M. W. Powers, "Evaluation: from precision, recall and F-measure to ROC, informedness, markedness and correlation," Oct. 2020, doi: 10.48550/arXiv.2010.16061.

[36] G. E. Hinton, N. Srivastava, A. Krizhevsky, I. Sutskever, and R. R. Salakhutdinov, "Improving neural networks by preventing co-adaptation of feature detectors," Jul. 2012, doi: 10.48550/arXiv.1207.0580.

Journal of Electronics, Electromedical Engineering, and Medical Informatics
Multidisciplinary: Rapid Review: Open Access Journal

Vol. 7, No. 2, April 2025, pp: 460-470; eISSN: 2656-8632

[37] C. Guo, M. Yu, and J. Li, "Prediction of Different Eye Diseases Based on Fundus Photography via Deep Transfer Learning," *J Clin Med*, vol. 10, no. 23, Dec. 2021, doi: 10.3390/JCM10235481.

[38] M. Jahnavi, D. Rajeswara Rao, and A. Sujatha, "A Comparative Study Of Super-Resolution Interpolation Techniques: Insights For Selecting The Most Appropriate Method," *Procedia Comput Sci*, vol. 233, pp. 504–517, Jan. 2024, doi: 10.1016/J.PROCS.2024.03.240.

[39] C. Kumar, A. Choudhary, G. Singh, and Ms. D. Gupta, "Enhanced Super-Resolution Using GAN," *Int J Res Appl Sci Eng Technol*, vol. 10, no. 5, pp. 2077–2080, May 2022, doi: 10.22214/IJRASET.2022.42718.

[40] R. Sarode, S. Varpe, O. Kolte, and L. Ragha, "Image Super Resolution using Enhanced Super Resolution Generative Adversarial Network," *ITM Web of Conferences*, vol. 44, p. 03054, 2022, doi: 10.1051/ITMCONF/20224403054.

[41] C. Ledig *et al.*, "Photo-Realistic Single Image Super-Resolution Using a Generative Adversarial Network," *Proceedings - 30th IEEE Conference on Computer Vision and Pattern Recognition, CVPR 2017*, vol. 2017-January, pp. 105–114, Sep. 2016, doi: 10.1109/CVPR.2017.19.

[42] O. Keles, M. A. Yilmaz, A. M. Tekalp, C. Korkmaz, and Z. Dogan, "On the Computation of PSNR for a Set of Images or Video," *2021 Picture Coding Symposium, PCS 2021 - Proceedings*, Apr. 2021, doi: 10.1109/PCS50896.2021.9477470.

[43] K. Yamashita and K. Markov, "Medical Image Enhancement Using Super Resolution Methods," *Computational Science – ICCS 2020*, vol. 12141, p. 496, 2020, doi: 10.1007/978-3-030-50426-7_37.

[44] H. Sajati, "The Effect of Peak Signal to Noise Ratio (PSNR) Values on Object Detection Accuracy in Viola Jones Method," *Proceeding SENATIK ITD Adisutjipto Yogyakarta*, vol. 4, no. 0, pp. 167–174, Nov. 2018, doi: 10.28989/SENATIK.V4I0.139.

[45] E. Yoshai, G. Goldinger, M. Haifler, and N. T. Shaked, "Super resolution of histopathological frozen sections via deep learning preserving tissue structure," Oct. 2023, doi: 10.48550/arXiv.1905.11946.

[46] K. Yamashita and K. Markov, "Medical image enhancement using super resolution methods," *Lecture Notes in Computer Science (including subseries Lecture Notes in Artificial Intelligence and Lecture Notes in Bioinformatics)*, vol. 12141 LNCS, pp. 496–508, 2020, doi: 10.1007/978-3-030-50426-7_37/FIGURES/9.

AUTHOR BIOGRAPHY

IDA MASLUHA is currently pursuing a Bachelor's degree in the Informatics Engineering study program at the University of Muhammadiyah Malang since 2021. Throughout her journey, Ida has actively developed an interest in the field of data science, including data processing, data analysis and data visualization. Apart from that, Ida is also active in expanding knowledge in the field of cyber security through academic and organizational activities on campus. Outside of her academic activities, Ida runs a small business in the field of photography, which combines her passion for visual arts with entrepreneurship. This combination of academic and non-academic activities reflects Ida's commitment to developing competencies and exploring potential in various fields of interest, both in the world of technology and the arts.

YUFIS AZHAR received his Bachelor's degree in Computer Science from the Informatics Engineering program at Universitas Muhammadiyah Malang in 2009, and his Master's degree in Computer Science from Institut Teknologi Sepuluh Nopember, Surabaya, in 2013. Currently, he is a lecturer at the Informatics Study Program at Universitas Muhammadiyah Malang. His research interests include computer vision and machine learning. He has published numerous papers in reputable international journals and conferences. He also serves as a reviewer for several indexed journals and is actively involved in academic collaborations. In addition to his academic work, he is involved in various research projects focused on the application of AI technologies in real-world problems.